The use of acoustic reflectors to enlarge the effective area of planar sensor arrays

R. Ellwood[1], E.Z. Zhang[1], P.C. Beard[1] & B.T. Cox[1]

[1]Department of Medical Physics and Bioengineering, University College London, WC1E 6BT. UK

ABSTRACT

Planar sensor arrays have many advantages including ease of manufacture and low cost. However, when used for photoacoustic (PA) imaging, planar sensors have a limited view of the acoustic field, which means some of the waves from the PA source are not recorded. This results in artifacts in the reconstructed image of the PA source (the initial acoustic pressure distribution). In this paper, we describe novel sensor array configurations based on the Fabry Perot (FP) sensor and acoustic reflectors that retain its detection advantages while improving the visibility of the reconstructed PA image.

Keywords: limited view, artifacts, planar sensor, Fabry-Perot sensor, Photoacoustic imaging, acoustic reflectors

1. INTRODUCTION

Planar sensor arrays, eg. interferometric optical sensors[1], or capacitive micromachined ultrasonic transducers (CMUTs)[2], are often easier to fabricate (or interrogate), than curved or spherical arrays, especially when small element sizes are required, such as in photoacoustic imaging. However, their planarity also leads to a disadvantage: a limited aperture detection which means that a proportion of the emitted photoacoustic waves (see Figure 1) are not captured. This is the so-called limited view problem and results in artifacts in the reconstructed image. These artifacts can appear as erroneous structures or can distort actual structure in an image. They can also affect the accuracy of quantitative photoacoustic tomography (PAT[3]).

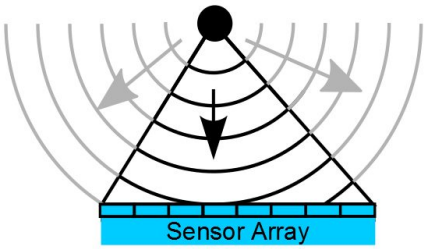

Figure 1 Image demonstrating the limited aperture problem. The limited aperture problem arises due to the finite size of the sensor. This means that parts of the acoustic field are not captured by the sensor.

This paper examines the use of multiple acoustic reflectors to increase the effective aperture by redirecting the sound field onto the sensor array. This allows recovery of parts of the image, for example edges that are close to vertical, that would otherwise be invisible.

Section 2 describes the use of acoustic reflectors to increase the effective aperture of the sensor. In section 3, numerical simulations of this technique are presented. An experimental configuration for implementing this technique based on an optically addressed planar Fabry Perot ultrasound sensor is introduced in section 4 and the result are presented in section 5. Finally a discussion of the limitations and practical capabilities of using acoustic reflectors to extend the effective aperture of the sensor is presented in section 6.

Photons Plus Ultrasound: Imaging and Sensing 2014, edited by Alexander A. Oraevsky, Lihong V. Wang,
Proc. of SPIE Vol. 8943, 89436A · © 2014 SPIE · CCC code: 1605-7422/14/$18 · doi: 10.1117/12.2039240

2. USING ACOUSTIC REFLECTORS TO EXTEND THE EFFECTIVE APPERTURE OF PLANAR SENSOR ARRAYS

Figure 2 illustrates the concept of using acoustic reflectors to extend the effective aperture of planar sensor arrays. An acoustically reflective cavity is formed by placing reflectors perpendicular to a planar sensor array. Acoustic wave fronts emitted by the photoacoustic source are reflected from the reflectors and directed onto the sensor array. In this way the wave fronts that are emitted at an angle that would have not been detected by the normal aperture of the detector, will be reflected onto the sensor and so detected. Other reflector geometries have been explored[4]. Perpendicular reflectors have the advantage of not requiring the full enclosure of the sample under investigation. It is assumed that the acoustic reflectors are 100% reflective (pressure reflection coefficient of 1).

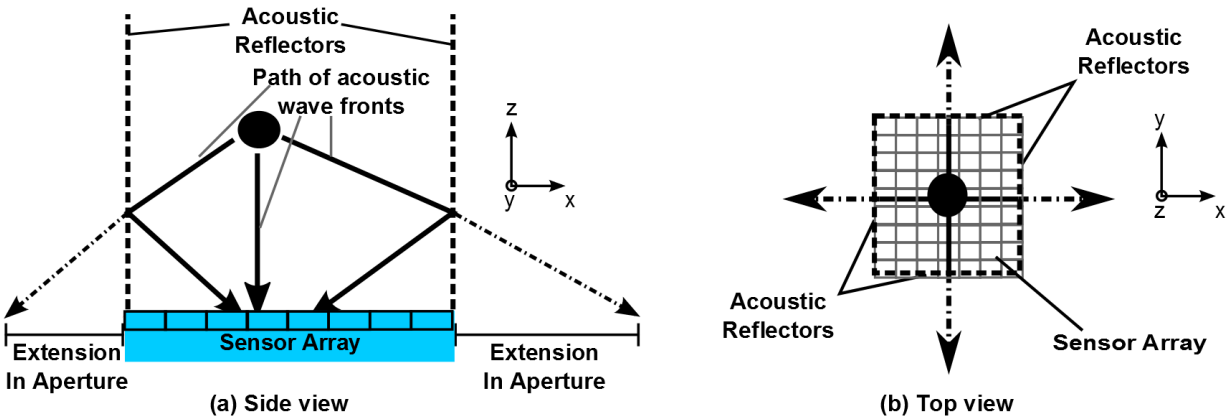

Figure 2 Diagram demonstrating the technique developed to extend the effective aperture of a planar sensor array by using acoustic reflectors that are perpendicular to the sensor surface. (a) shows a side view of the reflector geometry with arrows indicating the extension in the aperture due to the reflection. (b) shows a top view of this arrangement

2.1 Image reconstruction technique

In photoacoustic imaging, a spatially varying increase in pressure $p_0(x, y, z)$ follows the absorption and thermalisation of a pulse of light. As the tissue is elastic, this increase in pressure will propagate as an acoustic wave which is detected by the planar sensor array. If the coordinates are chosen so that the sensor array lies in the z=0 plane, then the detected data set comprises a series of spatially separated pressure time series $p(x, y, t)$, see Figure 3. The purpose of the image reconstruction is to map the measured data $p(x, y, t)$, back to the initial pressure field $p_0(x, y, z)$.

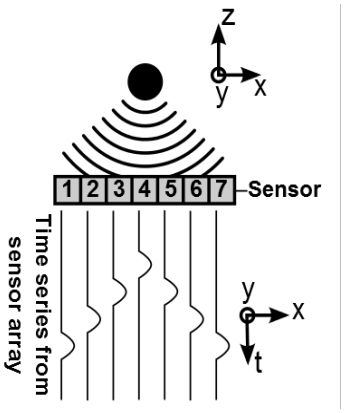

Figure 3 Initial pressure field $p_0(x, y, z)$, defined in 3 dimensions, will propagate as an acoustic wave in tissue and be recorded on a sensor array as a series of spatially seperated pressure time series, $p(x, y, t)$.

In this paper an exact and fast FFT-based (Fast Fourier Transform) image reconstruction algorithm is used. The algorithm implicitly assumes the initial pressure distribution (p_0) is infinitely periodic in the lateral dimensions. When used conventionally, with free-space measurements, ie. without reflectors, this is strictly not the case. In the presence of reflectors the periodicity can be exploited (see [5] for more details). Using reflectors that are perpendicular to the sensor can be regarded as introducing image sources, and thereby extending p_0 periodically. By matching the physical periodicity of the image sources with the periodicity inherent in the FFT in this way, it makes the FFT-based image reconstruction algorithm exact.

In order to apply the algorithm, the data measured by the sensor is extended periodically by mirroring it about one of its endpoints. This is achieved by placing a mirrored copy of the original time series data alongside the original time series data, and applying the reconstruction algorithm to the combined data set. For example in the 1 dimensional case, the time series data from sensors 1 to N that initially takes the form $p(1,2,3,\ldots,N)$ becomes $p(N,\ldots,3,2,1,1,2,3,\ldots,N)$.

The reflections from the walls could be considered as arrivals from image sources in the adjacent virtual imaged region. Due to reconstruction technique assuming a periodicity in the sensor data, the reflections from the virtual imaged region are mapped back onto the imaged region during the reconstruction (see Figure 4). In this way the reflections contribute to the reconstructed initial pressure field.

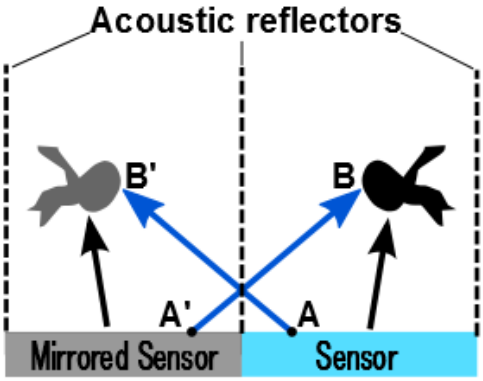

Figure 4 Diagram depicting how the reconstruction technique makes use of the reflected waves in the reconstruction to improve the reconstructed initial pressure field $p_0(x,y,z)$. Note that the ray depicted by the longer arrow would have taken a path that reflected from the walls as it propagated (B to A and B' to A'). However, the reconstruction algorithm assumes that the wave fronts have travelled in a straight path from the virtual sensor, next to the reconstruction, to the absorber (eg point A to B' and A' to B).

3. SIMULATIONS

Two 2D simulations were conducted to investigate the increase in the effective aperture that could be gained using perpendicular reflectors. In one simulation the reflectors were present. In the other simulation no reflectors were present. The simulations consisted of modelling the acoustic wave propagation and detection by a sensor array using a k-space pseudospectral time domain acoustic propagation model, k-Wave[6][7].

For the case where the reflectors were present the simulation was configured to allow reflections. The inherent periodicity of the FFT was exploited to simulate the reflections, by first mirroring the domain about its right hand edge (Figure 5). Data was only acquired from half of the domain. Absorbing boundary conditions were only applied to the top and bottom edges of the domain. For the simulation where no reflectors were present the waves were absorbed at the boundary of the computational domain, simulating free space propagation. The initial pressure distribution was reconstructed from the simulated data using a FFT-based reconstruction algorithm. Both simulations used a p_0 that was a 2D representation of the knotted tube phantom used experimentally, described in section 4.3, in order to facilitate qualitative comparison with the experimental results.

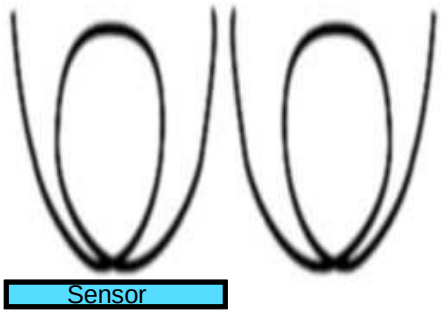

Figure 5 Image of the simulated phantom used when reflections are present. Note the mirrored copy on the right hand side. Due to the inherent periodicity of the FFT used in the acoustic forward model, and by collecting sensor data from only half of one side of the domain, this mirrored copy simulates the presence of reflections.

For both simulations a simulated signal to noise of 40dB and an acoustic attenuation coefficient 3dB $MHz^{-1}cm^{-1}$ was used. The acoustic field was recorded for a total 380μs. In the simulation where reflectors are present, the ratio of the sum of the acoustic pressure squared between the initial conditions and at the end of the simulation is 1.45×10^{-5}. The sum of the acoustic pressure squared is proportional to the amount of energy in the domain, so at the end of the simulation the majority of the energy has propagated out of the domain.

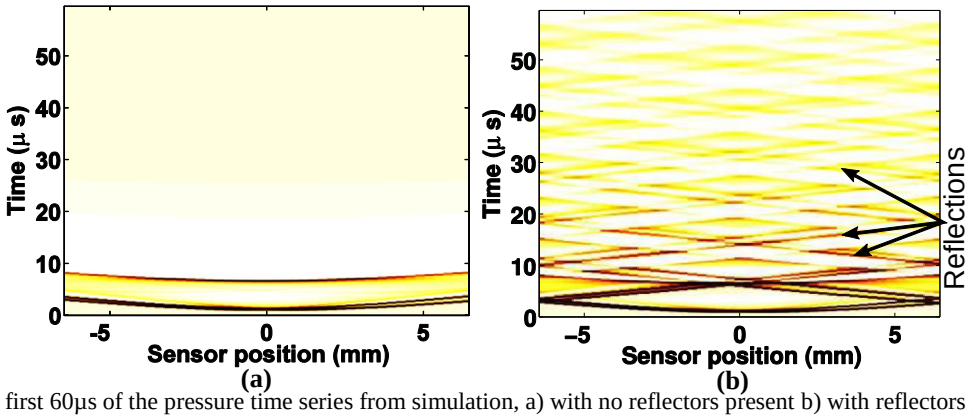

Figure 6 the first 60μs of the pressure time series from simulation, a) with no reflectors present b) with reflectors present. Note the reflections can be seen as a series of waves crossing the sensor surface.

The simulated time series over the first 60μs with and without reflections can be seen in Figure 6. In the time series reflections take the form of a series of wave fronts crossing over the sensor (see arrows in Figure 6).

Figure 7 shows the initial pressure distribution reconstructed from the simulated pressure time series in Figure 6. Both cases where no reflections are present (Figure 7(a)), and where reflections are present (Figure 7(b)) can be seen. Clearly there is an improvement in the image that includes the reflections; more of the true features are visible in the image, and there are fewer artifacts. These artifacts can be seen in the reconstruction without reflections as structure at the side of the loop where there is no structure in the simulated phantom (see dashed oval regions in Figure 7a). The visibility of features that are tending towards being perpendicular from the sensor is improved when reflections are used in the reconstructions.

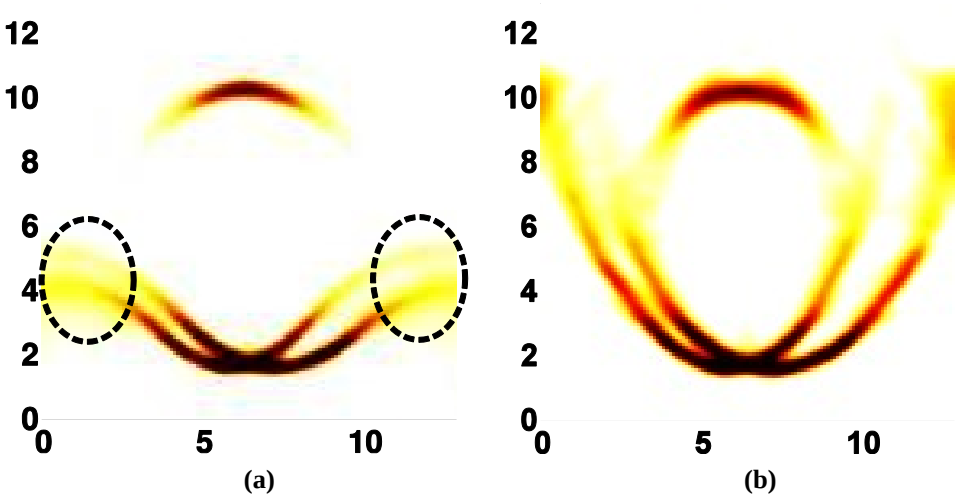

Figure 7 Reconstructed initial pressure distribution from 2D k-Wave simulations. a) Without reflections. b) With reflections. Note including reflections improves visibility of features more perpendicular to sensor. Artifacts are highlighted in (a) by dashed ovals.

4. EXPERIMENTAL CONFIGURATION

This section describes the experimental configuration used to investigate the use of perpendicular reflectors in extending the effective aperture of a sensor.

4.1 Reflectors

The reflectors consisted of 4 borosilicate crown (BK 7) glass prisms glued together to form a $1cm^3$ hollow cube faced with glass reflectors on the four vertical sides. This reflector arrangement was placed directly on the sensor surface. Prisms were used to avoid secondary wall reflections inside the glass complicating the reconstruction. Glass being optically transparent had the advantage that it allowed the direct illumination of the region of interest (using opaque reflectors makes is difficult to achieve an even distribution of light inside the cavity). A limitation of using glass is that it is not perfectly acoustically reflecting; based on a sound speed of $5660ms^{-1}$ for glass and $1482ms^{-1}$ for water[8], the pressure reflection coefficient $R = 0.81$. The reconstruction and simulation discussed in sections 2.1 and 3 assumed that the walls are 100% reflective, $R = 1$.

4.2 Imaging system

The acoustic sensor consisted of a 20µm thick Fabry-Perot (FP) polymer film sensor with -3dB bandwidth of approximately 40MHz[1]. The acoustic reflector was placed directly on top of the sensor. The photoacoustic signal was generated using a fibre coupled Q-Switched Nd:YAG laser with a pulse duration of 10ns, that was backward mode coupled into the system as shown in Figure 8.

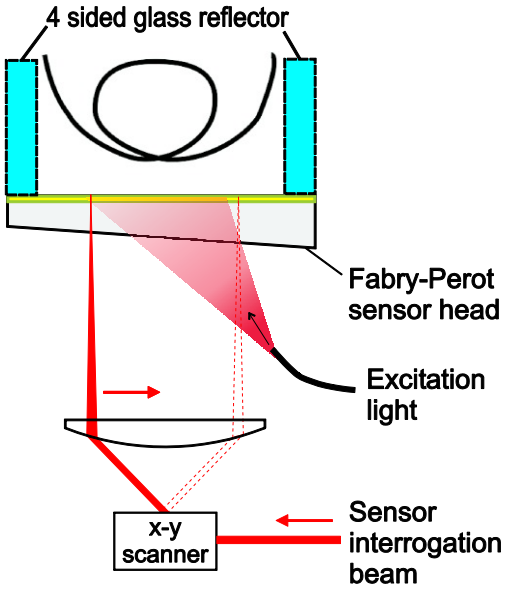

Figure 8 Diagram of experimental imaging set-up showing the phantom and acoustic reflector arrangement.

4.3 Phantom

The phantom used in this work consists of a tube (micro bore extension line, MX590, Smiths Medical) that was knotted (see Figure 9). This formed a loop, part of whose edges would be visible from the sensor (those parts close to parallel to the sensor) and part of which would not be (those parts close to perpendicular). This choice of phantom was made in order to demonstrate that including reflections will allow more of the edges to be reconstructed, corresponding to an effectively larger sensor aperture. The tube was filled with India ink diluted to 1% concentration, so that the illuminating light can penetrate throughout the diameter of the tube and not be solely absorbed at the surface.

Figure 9 Photo of the tube phantom used.

4.4 Experimental procedure

The phantom is placed inside the acoustically reflecting cavity, which is placed on top of the FP sensor and filled with deionized water. A scan area of 11mm by 12mm was selected, which deliberately overlaps the walls, so that the exact position of the walls can be obtained from the measured data. In this way the region of interest was defined, and measurements from outside this region were discarded pre-reconstruction. A step size of 100µm is used. By inspecting the time series it was found that the last reflections that were above the noise floor were observed at 22.6µs, this defined the length of each time series.

5. EXPERIMENTAL RESULTS

Reflections from the side walls of the reflector can be seen in the time series just as in the simulation (see arrows in Figure 10). To investigate the influence of a few reflections compared to many on the reconstructions, two reconstructions were produced corresponding to a short measurement time (very few reflections) and a longer measurement time (several reflections). To replicate the case where only a few reflections are present, data after $t_{max} = 6.8\mu s$ is removed, the data set is then zero padded and the transition between the data and the zeroes was smoothed using a Blackman window on the time series. This means that some reflections are still present but it approximates to the case where there are no reflecting walls. In the second reconstruction all of the data is used. Both cases are reconstructed in exactly the same way.

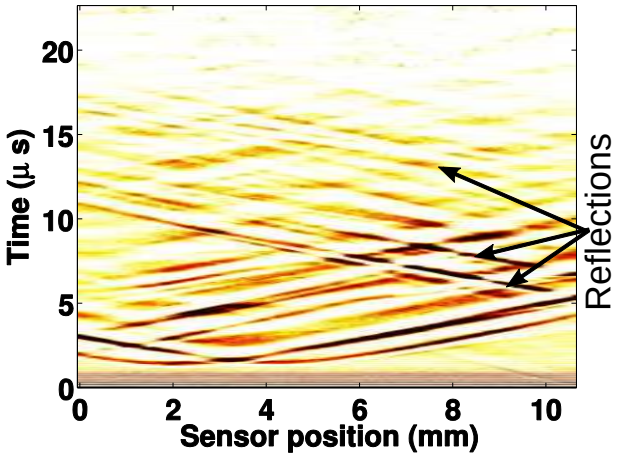

Figure 10 Measured pressure time series obtained using the phantom shown in figure 9. Note the reflections can be seen as a series of waves crossing the sensor surface, highlighted with arrows.

In Figure 11 maximum intensity projections (MIPs) of the reconstructions for both cases can be seen, rendered in Visualization Sciences Group Amira[9]. In the case where the data is reconstructed with all of the reflections present it can be seen that the rear loop of the tube and part of tube at a steep angle from the sensor is visible. In the case where fewer reflections are present these features are not clearly defined and there are more artefacts.

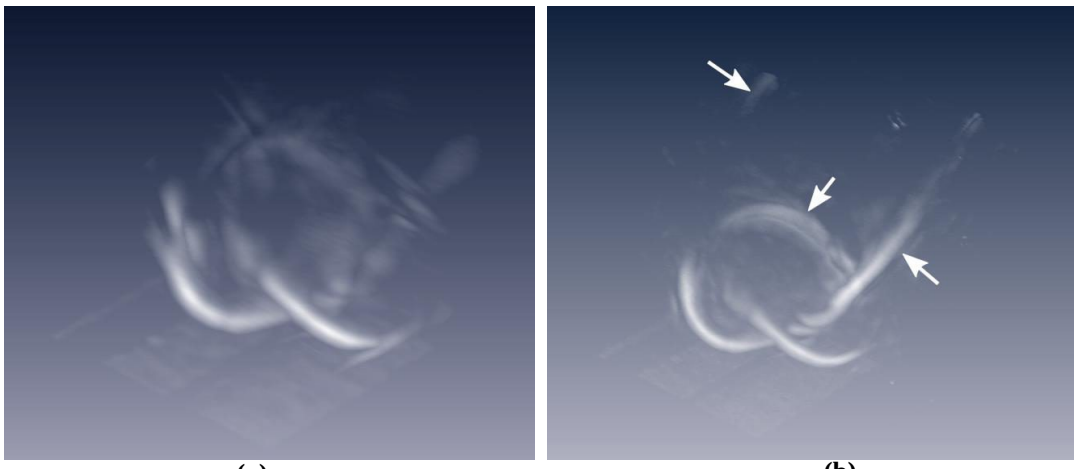

(a) **(b)**

Figure 11 Reconstructed initial pressure distribution displayed using Amira. a) With only a few reflections ($t_{max} = 6.8\mu s$). b) With all reflections ($t_{max} = 22.6\mu s$). Arrows in (b) highlight regions of improvement in reconstruction using more reflections.

5.1 Estimation of effective aperture

To give an estimate of how much the additional reflections increase the effective aperture, a 2D MIP of the loop in side profile is investigated. The aperture was defined as the distance between the intersections with the sensor of the lines drawn from the last well-reconstructed point on each of the reconstruction of the loop (see Figure 12). The case where only some of the reflections are present gives an effective aperture of 27.8mm, whereas the case where all the reflections are present gives an effective aperture of 39.1mm. This represents an increase in the linear aperture of 40%. Assuming that the cavity is perfectly symmetrical, both linear directions will see the same increase. This demonstrates an increase in the effective area of almost 100%.

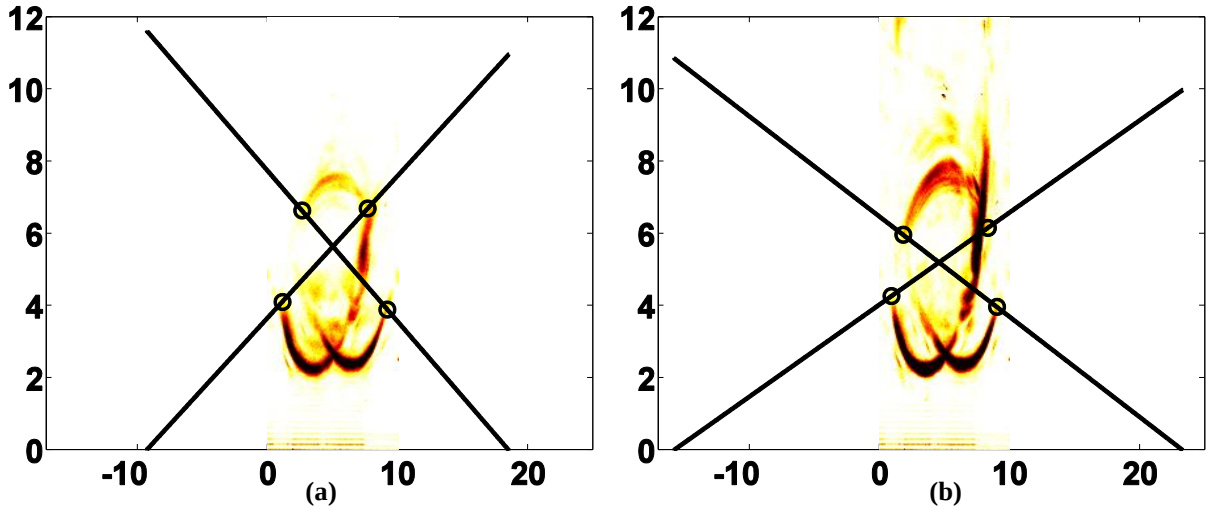

Figure 12 Maximum intensity projection (MIP) of reconstructed initial pressure distribution a) With only a few reflections ($t_{max} = 6.8\mu s$) - aperture length of 27.8mm. b) With all reflections ($t_{max} = 22.6\mu s$) - aperture length of 39.1mm. Black circles denote the last found reconstructed point. The lines are extrapolated from these points, where these lines reach zero (the location of the sensor) denotes the aperture length in this dimension.

6. DISCUSSION

Due to the nature of acoustic propagation, the ultrasonic pulses emitted by the photoacoustic source will propagate in all directions. This means that while the reflectors help in collecting more of this field than would have otherwise been collected, those parts travelling parallel or close to parallel to the sensor will not reach the sensor in time to be detected. Furthermore, because of the geometrical spreading (and absorption) that the waves undergo, the later arrivals will be reduced in amplitude. The proportion of the total pressure field that is collected is therefore further limited by the finite noise floor of the detector (~0.21kPa), with a proportion of the pressure field being below the noise threshold by the time it reaches the detector. So this reflector and sensor configuration, while offering an improvement over a planar sensor, still does not have a region where the initial pressure field is fully recoverable; there is no 'visible' region.

The uncertainty in the perpendicularity of the walls was estimated using digital calipers to be approximately 1º. This will affect the acoustic path of the reflected waves and so the location of their contribution to the final reconstruction. Higher frequencies and multiple reflections will be sensitive to this uncertainty.

Using glass for the acoustic reflectors means that the walls are not 100% acoustically reflective which is one of the assumptions in the reconstruction. The result is that the reflections are diminished and so too are their contribution to the final reconstruction. Using harder materials such as silicon carbide or tungsten, which have higher acoustic impedances, for the walls of the reflector would help but not solve this issue. However, using these materials would also complicate the illumination of the sample.

It should be noted that even with all of these practical limitations a clear improvement can be seen in the reconstruction of the acoustic field in the case where more reflections are used. This would indicate that this technique is resilient to the practical limitations discussed above and can be practically implemented to extend the aperture of planar sensors.

7. CONCLUSION

This paper has demonstrated experimentally that acoustic reflectors perpendicular to a planar sensor can be used to extend the effective detection aperture of these arrays, and thereby improve the quality of photoacoustic images. Extending the effective aperture allows acoustic waves that are travelling at steeper angles relative to the sensor plane to be acquired by the sensor, this allows the recovery of features in the initial pressure distribution that are not visible to the planar sensor alone. The estimated increase in effective aperture is ~40% in each direction. This increases the effective area of the sensor array by approximately 100%. Whilst this is a significant improvement, full view reconstructions are not possible using this technique. Using reflectors in this way is a cost-effective and easily implementable means of increasing the effective detection aperture of a planar array.

REFERENCES

[1] Zhang, E., Laufer, J. and Beard, P. C., "Backward-mode multiwavelength photoacoustic scanner using a planar Fabry-Perot polymer film ultrasound sensor for high-resolution three-dimensional imaging of biological tissues," Appl. Opt. 47(4), 561-577 (2008).

[2] Vaithilingam, S., Wygant, I. O., Kuo, X., Zhuang, P.S., Oralkan, O., Olcott, P. D. and Khuri-Yakub, B. T., "Capacitive Micromachined Ultrasonic Transducers (CMUTs) for Photoacoustic imaging," Proc. of SPIE 6086, 608603 (2006)

[3] Cox, B. T., Laufer, J. G., Arridge, S. R., and Beard, P. C. "Quantitative spectroscopic photoacoustic imaging: a review." Journal of Biomedical Optics, 17(6), 061202 (2012).

[4] Huang, B., Xia, J., Maslov, K. and Wang, L. V., "Improving limited- view photoacoustic tomography with an acoustic reflector," Journal of Biomedical Optics (Letters), 18(11), 110505-1-3, (November 2013)

[5] Cox, B. T., Arridge, S. R., and Beard, P. C., "Photoacoustic tomography with a limited- aperture planar sensor and a reverberant cavity," Inverse Problems, 23, 95-112 (2007)

[6] Treeby, B. E. and Cox B. T., "k-Wave: MATLAB toolbox for the simulation and reconstruction of photoacoustic wave fields," Journal of Biomedical Optics, 15(2), 021314-1-12 (March 2010)

[7] Treeby, B. E., and Cox, B. T. , "k-Wave Matlab toolbox," 2013, < http://www.k-wave.org/ > (12 February 2014), www.k-wave.org

[8] Kaye, G. W. C., and Laby, T. H., [Tables of physical and chemical constants], Longman, London & New York 29,30,74,76 (1986).

[9] Visualization Sciences Group "Amira visulisation software," 2013 <http://www.vsg3d.com/amira/overview> (12 February 2014), www.vsg3d.com/amira/overview